Korean J. Chem. Eng., 33(3), 1075-1079 (2016)
DOI: 10.1007/s11814-015-0262-0

pISSN: 0256-1115
eISSN: 1975-7220

Facile synthesis of bimetallic Ni-Cu nanoparticles using liquid phase plasma method

Seung Han Sun* **and Sang-Chul Jung****,†**

*Asia Pacific International School, Seoul 139-852, Korea
**Department of Environmental Engineering, Sunchon National University, Sunchon 57940, Korea
(*Received 29 August 2015 • accepted 26 November 2015*)

Abstract−A liquid phase plasma (LPP) process was used to synthesize of Ni-Cu bimetallic particles in aqueous solution. The bimetallic particles were well separated, and the particle size increased with increasing LPP process duration, causing these bimetallic particles to be well separated as the particle size increased when the LPP process time increased. The earliest stages of LPP formed dendrite-shaped nanoparticles, while spherical particles were generated in the later stages. While spherical Ni-Cu bimetallic nanoparticles were mostly observed in the initial stage, flower-like shaped Ni-Cu bimetallic nanoparticles were mostly observed after longer durations of plasma treatment. The solution pH decreased with increasing LPP process time.

Keywords: Liquid Phase Plasma, Bimetallic Nanoparticle, Nickel, Copper

INTRODUCTION

Nanoparticles of copper and nickel are widely used because they possess good catalytic activity. Ni particles have been used in catalytic cracking, whereas copper catalysts have been tested for NO reduction [1,2]. Nickel [3] and copper [4,5] particles have previously been applied as the anode materials in energy storage devices. In energy storage device applications, the use of multiple metals can result in enhanced properties compared to those of a single metal. Several methods have been proposed for the preparation of nickel and copper bimetallic particles in order to improve the properties of the resultant material.

Ni-Cu bimetallic compounds have been prepared by a variety of processes [6-9] and have been applied to catalysts for the production of hydrogen gas [10,11], reforming reactions [12], hydrogen addition [13,14], partial oxidation process [15], and cross coupling processes [16]. These studies have found that the Ni-Cu bimetallic composition controls the alloying and structure of Ni-Cu catalysts, which in turn influences their selectivity and activity [17].

The LPP process has received considerable attention in recent studies as it is a relatively simple process that allows for control of the size distribution and morphology of the particles [18,19]. The LPP Process is known to cause discharge in the liquid phase by exchanging electrons and ions in aqueous solution. The precursors of metal exist in the reactant solution, which are reduced by the electrons produced in the plasma field and then precipitated, forming metal particles. The LPP method can also generate metallic nanoparticles by the reduction of metal ions. This process has been recognized as one of the most effective methods for simple and accelerated synthesis of metal nanoparticles [20].

In our previous studies, we reported the synthesis of Ni [21] and Cu [22] nanoparticles using the LPP process. In the present study, the applicability of the LPP method to the synthesis of bimetallic particles was evaluated. Bimetallic Ni-Cu nanoparticles were synthesized using the LPP method, and the effects of a number of LPP process parameters on their synthesis were observed. The chemical and physical properties of the synthesized bimetallic Ni-Cu nanoparticles were examined by instrumental analysis.

EXPERIMENTAL METHODS

The configuration used for the LLP synthesis of bimetallic Ni-Cu nanoparticles dispersed in an aqueous solution is described in our previous studies [21,22]. The LPP experimental device consists of LPP reactor with electrodes, a power supply system which can control the pulsed discharge parameters, a reactant solution supply system, and a spectroscopic analysis system. Further details of the experimental device can be found in previous papers [21,22].

Nickel nitrate hexahydrate ($Ni(NO_3)_2{\cdot}6H_2O$, Sigma-Aldrich) and copper nitrate trihydrate ($Cu(NO_3)_2{\cdot}4H_2O$, Sigma-Aldrich) were used as the precursors of nickel and copper, respectively. Cetyltrimethylammonium bromide ($CH_3(CH_2)_{15}N(CH_3)_3Br$, CTAB, Daejung Chemical) was used to aid the uniform dispersion of bimetallic particles in aqueous solution, and ultrapure water (Daejung Chemical) served as the solvent.

The volume of LPP reaction solution was 250 ml. The concentrations of $Ni(NO_3)_2{\cdot}6H_2O$ and $Cu(NO_3)_2{\cdot}4H_2O$ were each 5 mM. CTAB with a 25% molar ratio with respect to total precursor quantity (2.5 mM) was added. The LPP process was prompted by applying pulsed-electric power to the tungsten electrodes. Coolant was circulated outside of the LPP reaction quartz reactor to maintain a constant temperature of LPP reaction solution. When the LPP reaction was completed, reactants and CTAB were removed from the solution through centrifugation and washing.

†To whom correspondence should be addressed.
E-mail: jsc@sunchon.ac.kr
‡The authors declare that there is no conflict of interests regarding the publication of this article.

The optical emission spectrum (OES) of the LPP discharged Ni-Cu nitrate reactant solution was recorded using an optical emission spectrometer (Avantes); a field emission transmission electron microscope (TECNAI-20, FETEM, FEI) was used to monitor the size, morphology, and the degree of dispersion of the generated bimetallic Ni-Cu nanoparticles. The morphology and size of the bimetallic Ni-Cu nanoparticles were then determined using a high resolution field emission transmission electron microscope (HR-FETEM, JEM-2100F, JEOL).

RESULTS AND DISCUSSION

Various chemical species are created in the liquid phase during the LPP process. To determine chemically active species which occur due to the plasma reaction, it is necessary to examine the effects of the chemical species. Chemical species in the liquid phase were determined during the LPP process by using an optical emission spectrometer. Fig. 1 shows the spectrum resulting from OES determinations during the LPP processing of the nickel-copper nitrate solution. The excited states of atomic nickel ($1s^2 2s^2 2p^6 3s^2 3p^6 3d^8 4s^2$ $^3F_4$, at 341.4, 346.1, 352.4, and 361.9 nm) and atomic copper ($1s^2 2s^2 2p^6 3s^2 3p^6 3d^{10} 4s$ $^2S_{1/2}$, at 324.8, 510.5, 515.2, and 521.8 nm) were detected in the emission spectra [23,24]. OES determinations suggest that nickel-copper ions were reduced to nickel-copper forming metal particles via the LPP reaction. The excited states of atomic H (H_β at 486 nm and H_α at 656 nm) and atomic O ($3p^5P \rightarrow 3s^5S^0$ at 777 nm), as well as the molecular bands of the hydroxyl radical OH (at 309 nm), were detected in the emission spectra [25,26]. The activated chemical species and radicals formed under high pressure during the process of LPP caused exceedingly expeditious reactions that provided excessive amount of data. The LPP process makes it possible to instantaneously form strong non-thermal plasma and also to produce a strong electric field that creates numerous chemically active species (OH*, O*, $^1O_2$, HO_2, O_2^-, H_2O_2, O_3, etc.) [27]. The application of LPP to a reactant solution is usually based on a spark discharge or a streamer discharge. When a spark discharge is used in the production of an electrical field, various free radicals, ozone and oxygen bubbling, overpressure shock waves, and strong ultraviolet radiation occur [28]. The production of activated chemical species in liquid solutions, such as hydroxyl radical, hydrogen peroxide and ozone, has been observed using a streamer corona pulsed discharge [29].

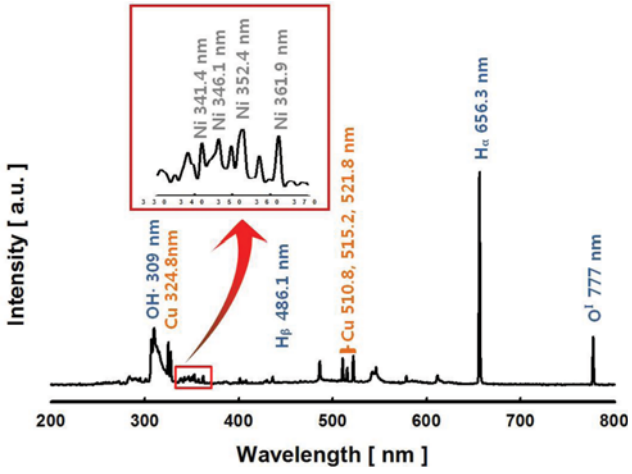

Fig. 1. Spatially and temporally integrated emission spectra for the pulsed electric discharge in nickel-copper nitrate solution.

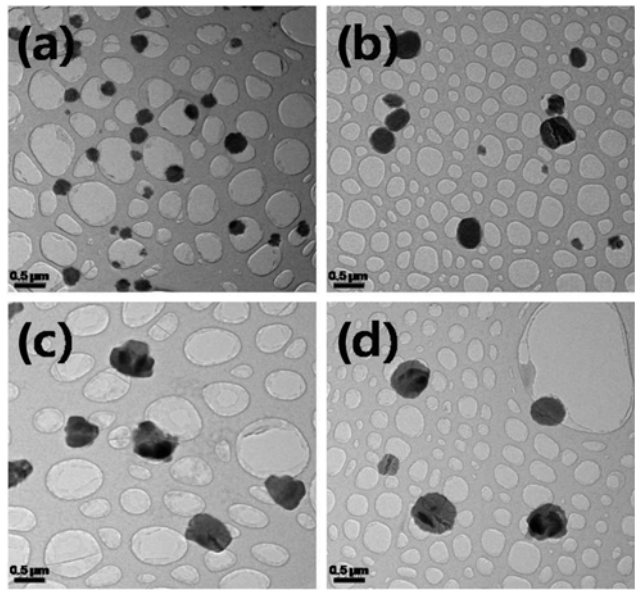

Fig. 2. HR-FETEM images of nanoparticles prepared by LPP process with different discharge times; (a) 5 min, (b) 10 min, (c) 20 min, (d) 30 min. All scale-bar is 0.5 μm.

Fig. 2 shows the HR-FETEM images of the metal nanoparticles observed after various LPP reaction durations. In all experiments, the precursor concentration of the LPP reaction solution was 5 mM and the surfactants (CTAB) ratio was 25%. The nanoparticle size increased with increasing LPP reaction duration. When the LPP reaction time was 5 min, nanoparticles were observed as well dispersed spherical-shaped particles with a size smaller than 50-200 nm. When the discharge time was 30 min, the particle size was increased to about 400-600 nm.

The elemental composition of the metallic particles generated from the application of nickel nitrate and copper nitrate to the

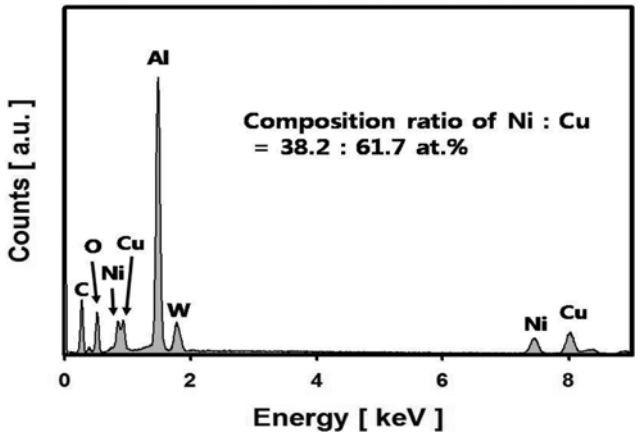

Fig. 3. EDS spectrum obtained of metallic nanoparticle by LPP process.

LPP process was examined. An aluminum holder was coated with the reactant solution that underwent the LPP reaction for 30 min, and energy dispersive spectroscopy (EDS) spectrum was carried out using FE-SEM (Fig. 3). The absorption peaks appearing at 1.48 and 1.77 keV are believed to stem from aluminum (Al) from the holder and tungsten (W) from the electrode. The absorption peak appearing at 0.28 keV is attributed to residual carbon (C) originating from the dispersant (CTAB). Nickel (Ni) was detected at 0.85 (Lα) and 7.47 (Kα) keV, whereas copper (Cu) was detected at 0.93 (Lα) and 8.04 (Kα) keV. These results indicate that both metal ions were formed during the LPP process using two metal precursors. The atomic ratio of Ni and Cu in the generated metallic particle was 32.8 : 61.7, containing more copper than nickel. The reduction reactivity of a metal is determined by its ionization tendency and normal potential. Among the transition metals, the standard potentials of nickel and copper are as follows:

$$Cu^{2+}(aq)+2e^{-}\rightarrow Cu(s)\ E^{0}=+0.34\ V \quad (1)$$

$$Ni^{2+}(aq)+2e^{-}\rightarrow Ni(s)\ E^{0}=-0.25\ V \quad (2)$$

Copper has a higher standard potential and a lower ionization tendency than nickel. Therefore, copper ions are preferentially reduced, leading to a higher copper content in the resulting particles. An oxygen (O) peak was observed at 0.52 keV, which is attributed to the oxidation of metal particles by active species ($^1O_2$, O_2^-, O•, OH•, HO_2, H_2O_2, O_3, etc.) formed during the LPP process. The oxygen content was determined to be 10-15 At% using EDX analysis, although this carries a relatively high degree of uncertainty as EDX does not analyze individual particles.

Fig. 4 shows the HR-FETEM images of nanoparticles, displaying nickel (red dots) and copper (green dots) which were generated using the LPP process. The particles were observed after 5 min LPP process duration, and particle size was determined to be about 100 nm. Spherical nanoparticles, such as those shown in Fig. 2, were observed. The element mapping image shows that a single nanoparticle contains both nickel and copper, indicating their bimetallic nature. The cobalt content (green dots) is greater than that of manganese (red dots), which is in agreement with the results of Fig. 3.

Fig. 5 shows HR-FETEM images of flower-like shaped bimetallic Ni-Cu nanoparticles created from the reactant solution. While spherical-sharped bimetallic Ni-Cu particles were mostly observed in the initial stage, anisotropic shaped and flower-like shaped

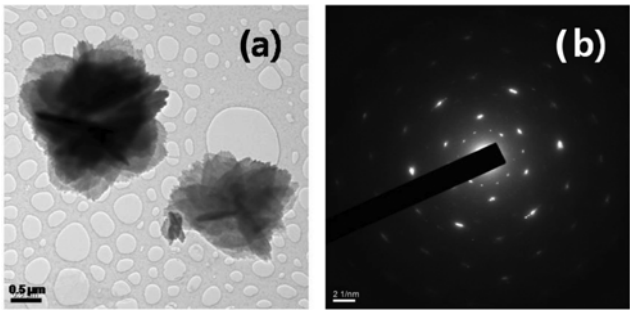

Fig. 5. HR-FETEM image of flower-like shaped Ni-Cu bimetallic nanoparticles (a) and corresponding nanoparticle ED patterns prepared by LPP process after 30 min.

bimetallic Ni-Cu nanoparticles were mostly observed after longer-term plasma-treated, as shown in Fig. 7. Guan et al. reported the synthesis of flower-like shaped nickel nanoparticles [30]. Spherical-shaped particles are created when the surface energies of crystal faces are equivalent to one another. This can also be described as the case for small particles when the surface energy does not depend on the crystal form, as the surface energy of particles increases depending on the crystal form. Fig. 5(b) shows the selected area diffraction pattern of the bimetallic Ni-Cu particles formed during the LPP process. The electron discharge pattern indicates that diffraction points are in accordance with the crystal of the lattice, as observed at various directions, indicating polycrystalline particles. Therefore, the diffraction points did not accomplish complete circles, indicating that individual nanoparticles are combined with much larger particles.

Fig. 6 shows the pH change of the nickel-copper nitrate aqueous solution as a function of LPP process duration. The solution pH steadily decreased during the plasma treatment. The reactive species formed during the LPP process, in particular H_α and H_β, induces the reduction of metal ions through various mechanisms, producing H^+ and reducing the pH of the solution [31].

$$Metal^{+}+H\bullet\rightarrow Metal^{0}+H^{+} \quad (3)$$

In addition, OES determinations (Fig. 1) showed that various oxidizing active species were generated through plasma reactions. It is supposed that the oxidizing active species reacted with nitrogen dissolved in the reactant solution to form nitric acid, leading to a

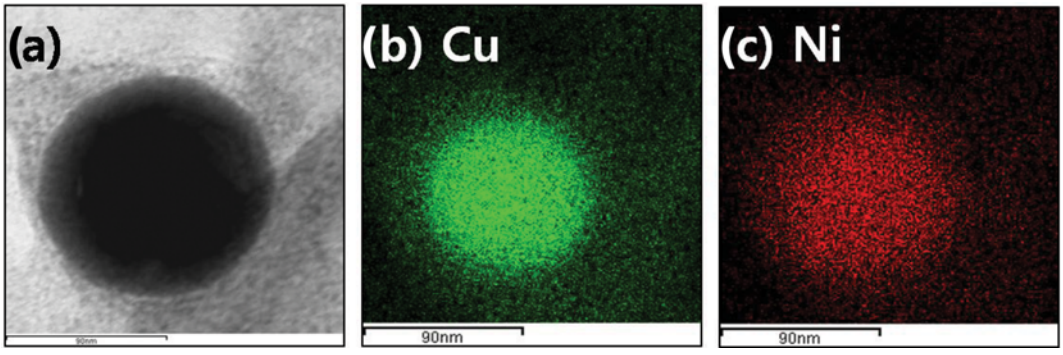

Fig. 4. HR-FETEM image of original particle (a) and elemental mapping (b), (c) of bimetallic Ni-Cu nanopartilces prepared by LPP process.

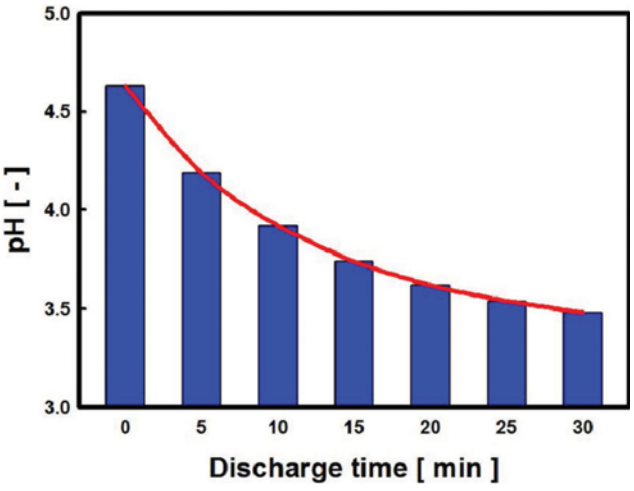

Fig. 6. Change in pH of the reactant solution as a function of LPP reaction time.

decrease in hydrogen exponent. The hydroxyl radicals produce hydrogen peroxide. The OH• are used for the reduction reaction to generate Ni-Cu particles. The role of oxidizing active species in the synthesis of metal particles in LPP process has been previously suggested based on electron spin resonance analysis [27].

A reaction for the preparation of Ni-Cu bimetallic particles with LPP method in liquid phase is proposed in Fig. 7. In the early stage, Cu^{2+} and Ni^{2+} are reduced, and dendrite particles are simultaneously synthesized. As the particles form during early stages, a nucleation reaction occurs. These particles are thought to be composed of clusters of nanoparticles with very small sizes. As the hydrogen ion concentration of the LPP reaction solution decreases with increasing LPP process time, Ni and Cu particles dissolve and become smaller. Because of the declining rate of reduction of Cu^{2+} and Ni^{2+}, Ni-Cu bimetallic particles with an anisotropic crystal form are generated in the LPP reactant, while spherical-shaped particles continue to dissolve in reactant solution. It has been suggested that the dissolution of Ni-Cu bimetallic particles depends on the specific crystal form. Tsuji reported the crystal form-selective etching of particles prepared by reduction reaction [32]. In this study, spherical-shaped particles dissolved, whereas decahedral and triangular particles continued to grow. The etching process occurs at the surface of particles surface with a high radius curve, and provides an initial guideline which might be used to reduce the size of particles of a specific crystal form [33].

CONCLUSION

A series of experiments involving LPP process evaluations were conducted to apply the LPP process for synthesis of Ni-Cu bimetallic nano-particles. The conclusions are as follows:

1. The excited states of atomic nickel, copper, hydrogen, and oxygen as well as the molecular bands of the hydroxyl radical were detected in the emission spectra for the discharge in the reactant solution.
2. Spherical shaped Ni-Cu bimetallic nanoparticles were well dispersed and the particle size was increased with increasing LPP process time.
3. When the content of copper and nickel in the precursor was the same, copper nanoparticles were preferentially precipitated.
4. The generated Ni-Cu bimetallic nanoparticles had a polycrystalline structure. The atomic % composition of the particles was shown to be about 30% Ni, 60% Cu, and 10% oxygen.

While spherical Ni-Cu bimetallic nanoparticles were mostly observed in the initial stage, flower-shaped Ni-Cu bimetallic nanoparticles were mostly observed after longer plasma treatment.

REFERENCES

1. R. Aiello, J. E. Fiscus, H. C. zur Loye and M. D. Amiridis, *Appl. Catal. A: Gen.*, **192**, 227 (2000).
2. P. Bera, S. T. Aruna, K. C. Patil and M. S. Hegde, *J. Catal.*, **186**, 36 (1999).
3. T. Hibino, A. Hashimoto, T. Inoue, J.-I. Tokuno, S.-I. Yoshida and M. Sano, *Science*, **288**, 2031 (2000).

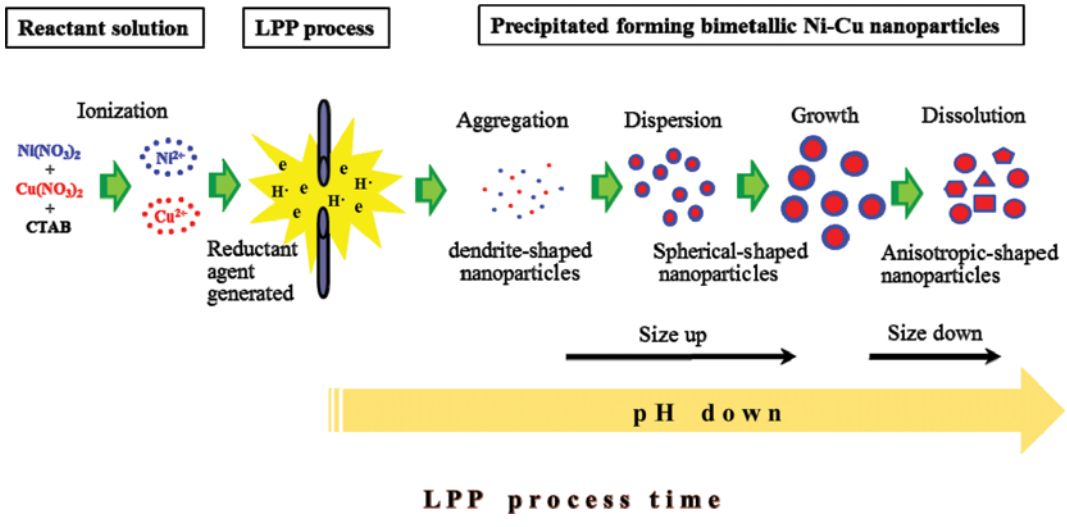

Fig. 7. Formation mechanism of Ni-Cu bimetallic nanoparticles synthesized with plasma in the liquid phase.

4. B. Khodashenas and H. R. Ghorbani, *Korean J. Chem. Eng.*, **31**, 1105 (2014).
5. S. Park, J. M. Vohs and R. J. Gorte, *Nature*, **404**, 265 (2000).
6. N. Rahemi, M. Haghighi, A. A. Babaluo, M. F. Jafari and S. Allahyari, *Korean J. Chem. Eng.*, **31**, 1553 (2014).
7. J. Feng and C.-P. Zhang, *J. Colloid Interface Sci.*, **293**, 414 (2006).
8. M. D. Cangiano, A. C. Carreras, M. W. Ojeda and M. D. Ruiz, *J. Alloys Compounds*, **458**, 405 (2008).
9. K. J. Carroll, J. U. Reveles, M. D. Shultz, S. N. Khanna and E. E. Carpenter, *J. Phys. Chem. C*, **115**, 2656 (2011).
10. H. Wang and R. T. K. Baker, *J. Phys. Chem. B*, **108**, 20273 (2004).
11. L. De Rogatis, T. Montini, B. Lorenzut and P. Fornasiero, *Energy Environ. Sci.*, **1**, 501 (2008).
12. T.-J. Huang and S.-Y. Jhao, *Appl. Catal. A: Gen.*, **302**, 325 (2006).
13. E. Asedegbega-Nietob, B. Bachiller-Baeza, A. Guerrero-Ruiz and I. Rodriguez-Ramos, *Appl. Catal. A: Gen.*, **300**, 120 (2006).
14. P. Li, J. Liu, N. Nag and P. A. Crozier, *J. Catal.*, **262**, 73 (2009).
15. A. Yin, C. Wen, X. Guo, W.-L. Dai and K. Fan, *J. Catal.*, **280**, 77 (2011).
16. B. H. Lipshutz, D. M. Nihan, E. Vinogradova, B. R. Taft and Z. V. Bŏskovic, *Organic Lett.*, **10**, 4279 (2008).
17. L. Guczi, *Catal. Today*, **101**, 53 (2005).
18. H. Lee, S. H. Park, S. C. Jung, J. J. Yun, S. J. Kim and D. H. Kim, *J. Mater. Res.,* **28**, 1105 (2013).
19. H. Lee, S. H. Park, S. J. Kim, Y. K. Park, B. H. Kim and S. C. Jung, *Microelectronic Eng.*, **126**, 153 (2014).
20. D. J. Lee, S. J. Kim, J. Lee, H. Lee, H. G. Kim and S. C. Jung, *Sci. Adv. Mater.*, **6**, 1599 (2014).
21. H. Lee, M. Chung, H. G. Ahn, S. J. Kim, Y. K. Park and S. C. Jung, *International Journal of Precision Engineering and Manufacturing*, **16**, 1305 (2015).
22. H. Lee, S. H. Park, S. G. Seo, S. J. Kim, S. C. Kim, Y. K. Park and S. C. Jung, *Current Nanoscience,* **10**, 7 (2014).
23. J. E. Sansonetti and W. C. Martin, *J. Phys. Chem. Reference Data*, **34**, 1559 (2005).
24. U. Litzén, J. W. Brault and A. P. Thorne, *Physica. Scripta.*, **47**, 628 (1993).
25. P. Pootawang, N. Saito and O. Takai, *Thin Solid Films*, **519**, 7030 (2011).
26. Š. Potocký, N. Saito and O. Takai, *Thin Solid Films*, **518**, 918 (2009).
27. N. Saito, J. Hieda and O. Takai, *Thin Solid Films*, **518**, 912 (2009).
28. P. Baroch, V. Anita, N. Saito and O. Takai, *J. Electrostatics*, **66**, 294 (2008).
29. B. Sun, M. Sato, A. Harano and J. S. Clements, *J. Electrostatics*, **43**, 115 (1998).
30. J. Guan, L. Liu, L. Xu, Z. Sun and Y. Zhang, *CrystEngComm*, **13**, 2636 (2011).
31. O. Takai, *Pure and Appl. Chem.*, **80**, 2003 (2008).
32. M. Tsuji, N. Miyamae, M. Hashimoto, M. Nishio, S. Hikino, N. Ishigami and I. Tanaka, *Colloids and Surfaces A: Physicochemical and Engineering Aspects*, **302**, 587 (2007).
33. J. Rodrguez-Fernndez, J. Prez-Juste, P. Mulvaney and L. M. Liz-Marzn, *J. Phys. Chem. B*, **109**, 14257 (2005).